Available online at www.sciencedirect.com
ScienceDirect
Trans. Nonferrous Met. Soc. China 34(2024) 2342−2353
Transactions of Nonferrous Metals Society of China
www.tnmsc.cn

Bio-dissolution and kinetics of pyrite-bearing waste ores in presence of *Acidithiobacillus ferrooxidans*

Mao-xin HONG[1,2], Jun WANG[1,2], Bao-jun YANG[1,2], Yang LIU[1,2], Rui LIAO[1,2], Shi-chao YU[1,2], Shi-tong LIU[1,2], An-ni TANG[1,2], Wei WANG[1,3], Guan-zhou QIU[1,2]

1. School of Minerals Processing & Bioengineering, Central South University, Changsha 410083, China;
2. Key Laboratory of Biohydrometallurgy, Ministry of Education, Central South University, Changsha 410083, China;
3. South China Institute of Environmental Sciences, Ministry of Ecology and Environment, Guangzhou 510655, China

Received 3 March 2023; accepted 26 September 2023

Abstract: Bioleaching treatment was used to decontaminate pyrite-bearing waste rocks, mitigating the risk of acid mine drainage (AMD) generation at source. The bioleaching results showed that nearly 82% of Fe and S could be removed from pyrite-bearing waste within 40 d in the presence of *Acidithiobacillus ferrooxidans* (*A. ferrooxidans*). Kinetics study showed that the removal of pyrite from waste ore was mainly in the control of the chemical reaction and internal diffusion. The results of X-ray diffraction (XRD) and X-ray photoelectron spectroscopy (XPS) indicated that the formed biogenic jarosite could passivate the residual pyrite under the mediation of *A. ferrooxidans*. Secondary bioleaching experiments on the residual samples revealed no noticeable decrease in solution pH and only 8 and 160 mg/L of iron dissolved from the two residual mine waste samples, respectively, indicating that the acid and iron release capacity of the mine waste samples was weakened.

Key words: acid mine drainage; pyrite; bioleaching; mine waste; jarosite; bio-passivation

1 Introduction

Acid mine drainage (AMD) is considered a global environmental problem encountered by the mining industry and the environmental protection sector because of its extremely low pH (less than pH 3) and elevated concentrations of hazardous heavy metals (e.g., Cd, Cu, Fe, Mn, Pb, and Zn) and toxic metalloids (e.g., As and Se) [1,2]. The discharge of untreated AMD into the water environment will cause acidification and heavy metal contamination of nearby water bodies and arable land, ultimately posing a threat to animal and human health through the food chain [3]. It is currently believed that the formation of AMD is mainly related to pyrite (FeS_2) [4]. Pyrite is the most widely distributed sulfide mineral in the Earth's crust, and it is usually found in association with other minerals such as copper, zinc, and coal [5]. In the mining and beneficiation of these minerals, pyrite, however, frequently ends up as gangue in tailings or waste rock due to its limited commercial value. For instance, it is estimated that hundreds of millions of tons of pyrite-bearing waste are generated annually due to the grinding, blasting, and crushing of ore in Canada [6]. Large amounts of exposed pyrite-bearing waste ores not only occupy a lot of lands but also easily come into contact with oxygen and surrounding water bodies (such as streams, groundwater and stormwater) to produce AMD [1,7].

The exposed pyrite is initially oxidized by O_2 and releases Fe^{2+}, SO_4^{2-}, and H^+ [8]. Under

Corresponding author: Bao-jun YANG, Tel: +86-13974885694, E-mail: yangbaojun0312@126.com
DOI: 10.1016/S1003-6326(24)66545-3

oxidizing conditions, Fe^{2+} is further oxidized to Fe^{3+}. The dissolution of pyrite will be significantly enhanced by the oxidation of Fe^{3+} [9]. However, the regeneration from Fe^{2+} to Fe^{3+} is sluggish, especially under acidic conditions [3]. In the natural environment, though acidophilic micro-organisms (such as *Acidithiobacillus ferrooxidans* (*A. ferrooxidans*)) are ineluctably involved in the dissolution of pyrite and enhance the oxidation of Fe^{2+} to Fe^{3+} [10], the overall process of pyrite oxidation is still relatively slow due to the low concentration of natural bacteria. AMD will generate continually as long as the exposed pyrite is not totally oxidized or passivated. As a result, AMD remediation takes a long time to complete and the operating system is normally expensive. For example, the total cost of AMD remediation in the world's four largest mining countries is expected to be US$ 3.2×10^8−7.2×10^9 [11].

Bioleaching is a well-established technology and is conventionally used to enhance the dissolution of metallic ores and recover valuable metals by artificially cultivating high concentrations of leaching bacteria [12−16]. Recently, the application of bioleaching in the decontamination of mine waste also appears to be a compelling attempt [17]. MÄKINEN et al [18] used mixed mesophilic bacteria for bioleaching of pyrite-bearing tailings and the results showed that 51% of Co, 100% of Zn, 69% of Cu and 59% of Fe could be removed after 10 d. Similarly, in another study, maximum Zn and Fe removals of 95.45% and 83.98%, respectively, were achieved after 25 d of bioleaching of lead−zinc mine tailings in the presence of *A. ferrooxidans* [19]. It is worth noting that published work on the use of bioleaching to decontaminate mine waste is mainly focused on pyrite-bearing tailings, while the aspect of pyrite-bearing waste rocks is rarely reported. Besides, even though many reports have been made on the bioleaching of pure pyrite [20], the bio-dissolution behavior and kinetics of pyrite during bio-removal from waste ore are unclear and further studies are needed due to the complex composition of actual waste rock.

Therefore, the purposes of this study are to (1) use bioleaching to decontaminate exposed pyrite-bearing waste ore, reducing the risk of AMD generation at source and (2) provide a solution for low-cost disposal of mine waste rocks. In this research, bioleaching was performed on three mine waste samples obtained from an AMD contamination site (Shaanxi province, China) in the presence of *A. ferrooxidans*. Scanning electron microscopy (SEM), X-ray diffraction (XRD) and X-ray photoelectron spectroscopy (XPS) were performed to reveal the mechanism during the process. Secondary release tests of leaching residues were conducted to verify the removal effect of pyrite.

2 Experimental

2.1 Minerals

Three mine waste samples (named MW1, MW2 and MW3, respectively) were collected from an AMD contaminated site in Shaanxi province, north-west China (Figure S1 in Supporting Information (SI)). All samples were ultrasonically cleaned with deionized water three times in order to remove the mud and other impurities. Samples were ground and sieved to a particle size of 38−74 μm after air drying naturally at room temperature for subsequent measurements and experiments. The chemical elemental analysis results showed that MW1 contained 2.68% Fe, 2.56% S, 45.30% O and 21.86% Si, and MW2 contained higher contents of 14.42% Fe and 13.12% S (Table S1 in SI). Among the three samples, the largest iron and sulfur content was observed in MW3, with 25.93% Fe and 22.88% S. X-ray diffraction (XRD) was used to identify the mineral phase in three mine waste samples, and the results are shown in Fig. S2 in SI. Major mineral compositions in MW1 were quartz (SiO_2), clinochlore ($(Mg,Fe^{2+})_5[Al_2Si_3O_{10}](OH)_8$), dolomite ($CaMg(CO_3)_2$), muscovite ($KAl_2(AlSi_3O_{10})(OH,F)_2$) and gypsum ($CaSO_4\cdot2H_2O$). In addition to peaks of quartz, clinochlore and muscovite, characteristic peaks of pyrite were also found in the XRD patterns of MW2. In contrast, the XRD pattern of MW3 showed the strongest pyrite peaks among other samples with relatively weak quartz and muscovite intensities. The results of XRD showed that the order of pyrite content in the three samples was as follows: MW1<MW2<MW3.

2.2 Strains and culture conditions

A. ferrooxidans ATCC 23270 strain used in this study was provided by the Key Lab of

Biohydrometallurgy, Ministry of Education, Central South University (China). The bacteria were aerobically cultivated at 30 °C and 170 r/min in 9K medium that consisted of $(NH_4)_2SO_4$ 3.0 g/L, $K_2HPO_4·3H_2O$ 0.5 g/L, $MgSO_4·7H_2O$ 0.5 g/L, KCl 0.1 g/L, $Ca(NO_3)_2$ 0.01 g/L and $FeSO_4·7H_2O$ 44.7 g/L. Dilute sulfuric acid of 0.1 mol/L was used to adjust initial pH of the medium to 2.0. Prior to centrifugation, the bacteria in the mid-exponential growth phase were initially filtered through a Whatman 42 filter paper to remove precipitates and metabolites. Then, the cell suspension was centrifuged in a centrifuge (Beckman Coulter, Inc. Avanti j-E) at 14400*g* and 4 °C for 15 min to remove the supernatant and obtain cell pellets. In order to obtain metabolite-free cells, the original cell pellets were washed with sterile iron-free 9K medium (pH=2) and recentrifuge three times. The metabolite-free cells were then resuspended and diluted in a sterile iron-free 9K medium (pH=2) for subsequent bioleaching experiments.

2.3 Bioleaching experiments

Firstly, bioleaching batch experiment of three mine waste samples was carried out in 250 mL flasks containing 99 mL sterile iron-free 9K medium, 1 mL concentrated metabolite-free cells of *A. ferrooxidans* and 2 g mine waste samples for 40 d. The initial pH was set to be 2.0, which was suggested as the optimal growth pH for *A. ferrooxidans* [21]. Initial inoculum concentration of *A. ferrooxidans* was 1.0×10^7 cell/mL. The shake flasks were placed in a rotary shaker at 30 °C and 170 r/min. Batch experiment was carried out in triplicate under the same conditions to guarantee the dependability of the experimental results. At the end of batch experiment, the residues were filtered through Whatman 42 filter paper and washed with deionized water for three times prior to vacuum drying for subsequent analyses and AMD release risk experiments of leached residues.

The risk for secondary AMD release of three leached residues was investigated by another bioleaching experiment. It was conducted in 250 mL flasks containing 1 g leached residues and 50 mL sterile iron-free 9K medium for 56 d with initial pH of 2.0 adjusted by 1 mol/L H_2SO_4, inoculation of 1.0×10^7 cells/mL, temperature of 30 °C and rotational speed of 170 r/min. The batch experiment was performed in duplicate under the same conditions to increase the reproducibility.

In all bioleaching experiments, deionized water was added to supplement the evaporation loss, while an iron-free 9K medium with a pH of 2.0 was added to the system to offset the sampling loss. During the experiment, 200 μL solution samples were regularly extracted as well as pH, oxidation−reduction potential (ORP), cell and iron concentrations were measured.

2.4 Analytical techniques

The concentrations of iron ions in the solution were determined by *o*-phenanthroline spectrophotometry and the correlation coefficient R^2 of the standard curve was greater than 0.999. Chemical element analysis of mineral samples was carried out with X-ray fluorescence (XRF), using an X-ray fluorescence S4 Explorer spectrometer (Bruker AXS, Germany). The number of free cells was counted using optical microscopy (CX31) with a hemocytometer (MUHWA Scientific MH−805142, China). A pH meter (PHS−3C) and an ORP meter (BPP−922) were used to measure the pH value and the ORP value of the solution, respectively. The residues after bioleaching were filtered through Whatman 42 filter paper, then rinsed with deionized water three times and dried in a vacuum drying oven (DZF−6050) for analysis. The component phase and surface morphology of the pristine samples and leached residues were examined using X-ray diffractometer (Bruker D8, Germany) and scanning electron microscope (Quanta 650 FEG), respectively. The X-ray photoelectron spectroscopy (XPS) analyses were conducted by a Thermo Fisher Scientific ESCALAB 250Xi photoelectron spectrometer. The C 1s with binding energy at 284.8 eV was used for calibration. Due to spin-orbit splitting, the 2p peak of Fe and S existed in the form of a double peak (Fe $2p_{3/2}$, Fe $2p_{1/2}$, S $2p_{3/2}$ and S $2p_{1/2}$), and the peak intensity of Fe/S $2p_{3/2}$ was twice that of the Fe/S $2p_{1/2}$ peak. The splitting energies of the spin-orbit doublets of Fe and S were 13.6 and 1.2 eV, respectively. The Gaussian–Lorentzian function was used for fitting the Fe and S 2p spectrum. The background fitting was performed using the Smart method. Only Fe/S $2p_{3/2}$ peaks were shown in the figures in order to simplify the graph.

3 Results and discussion

3.1 Bio-dissolution of pyrite from waste rocks

Variations in iron dissolution, solution pH, ORP and cell concentration during bioleaching of three mine waste samples for 40 d are shown in Fig. 1. According to the results of XRD (Fig. S2 in SI), Fe in MW2 and MW3 is mainly present in the pyrite; therefore, it is reasonable to use the dissolution of iron to judge the removal of pyrite in wastes roughly. Iron dissolution in MW1 remained constant at zero during the whole period of bioleaching (Fig. 1(a)), which meant that Fe in MW1 was insoluble and it possibly existed in the crystal structure of clinochlore [22]. In comparison, iron gradually dissolved from MW2 and MW3 and iron removal could reach around 82% after bioleaching for 40 d. As a result, most of the pyrite in the waste rocks was removed, which could significantly reduce the release of AMD into the environment at source. The solution pH of MW1 soared from an initial 2.0 to 6.5 within 2 d and then remained constant at around 6.1 during the period of bioleaching (Fig. 1(b)), which was related to the presence of acid-consuming substances in MW1, such as dolomite. MW2 and MW3 showed the same variations in pH with a gradual decline from an initial 2.0 to approximately 1.3 as the dissolution of pyrite was suggested as an acid-producing process [23].

The solution redox potential in the sulfides bioleaching system was suggested to be mainly determined by the concentration ratio of ferric ion to ferrous ion, and could be justifiable by the Nernst equation (Eq. (1)) [24]:

$$\varphi=\varphi^{0}+\frac{RT}{F}\ln\left(\frac{C_{Fe^{3+}}}{C_{Fe^{2+}}}\right) \tag{1}$$

where φ is the reaction potential (mV), φ^0 is the standard electrode potential (mV), T is the temperature (K), R is the molar gas constant equal to 8.314 J/(K·mol), F is the Faraday's constant and equal to 96.485 C/mol. ($C_{Fe^{3+}}/C_{Fe^{2+}}$) is the ratio between the concentrations of ferric and ferrous ions.

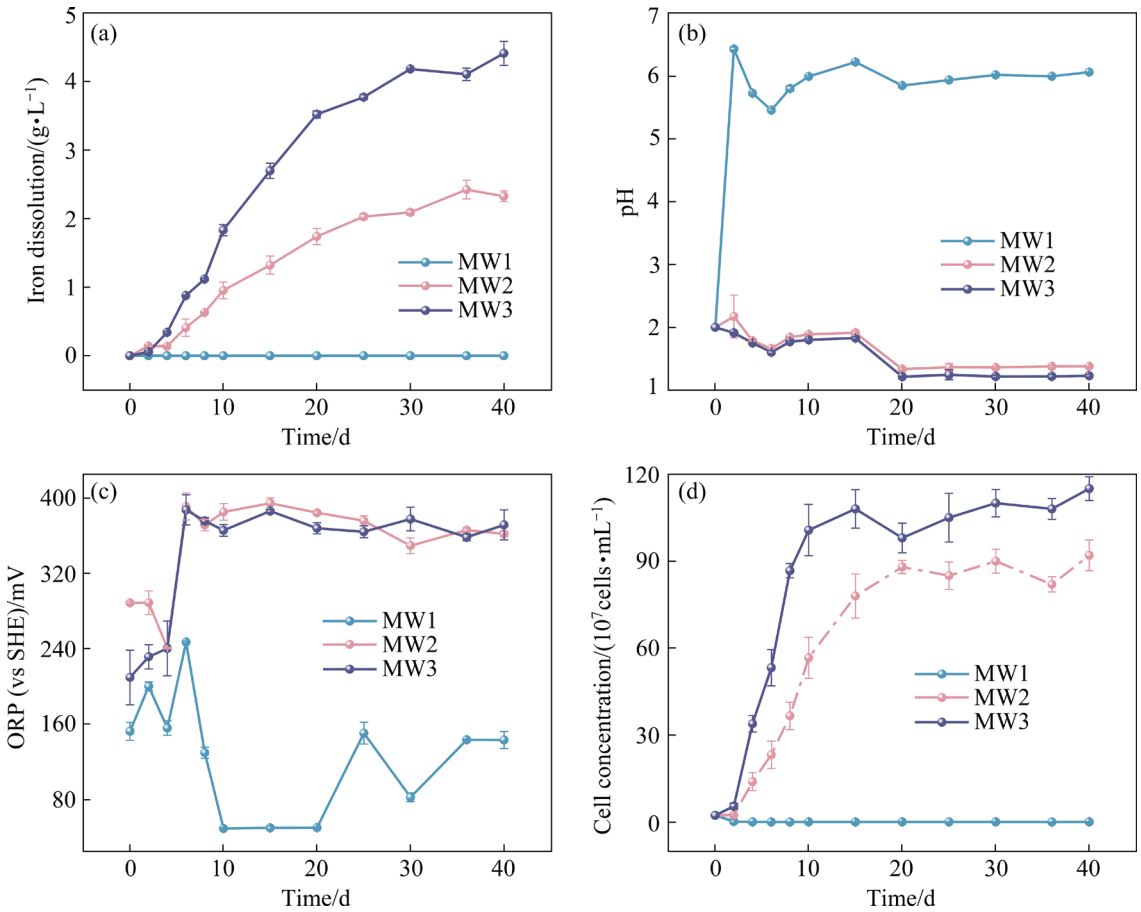

Fig. 1 Variations in iron dissolution (a), pH (b), ORP (c) and cell concentration (d) during bioleaching of three mine waste samples for 40 d in presence of *A. ferrooxidans*

The solution of ORP in MW1 fluctuated around 105 mV (vs SHE) throughout the leaching period (Fig. 1(c)). The solution of ORP in MW2 and MW3, however, dramatically increased to over 355 mV on Day 6 and remained at this level thereafter, which attributed to the oxidation of Fe^{2+} to Fe^{3+} by *A. ferrooxidans*. The bacterial concentration of MW1 decreased from initial inoculation level to hardly detected level within 2 d until the end of leaching (Fig. 1(d)). The suggested pH range of *A. ferrooxidans* was 1.3−3.5 [25]. Thus, the sharp increase in pH was detrimental to the growth and reproduction of bacteria. The bacterial concentrations of MW2 and MW3 rapidly increased to 8.0×10^8 cells/mL and 1.0×10^9 cells/mL, respectively, on the 15th day. Because of the higher content of iron and sulfur in MW3 (Table S1 in SI), bacterial growth and reproduction were better.

3.2 Kinetics study

The kinetics of pyrite removal from mine waste samples during bioleaching process was studied by using the shrinking-core model (Fig. 2), which is often used to analyze the kinetics data for mineral particles that are usually considered spherical particles [26]. According to the theories with different rate-controlling steps, the copper extraction and reaction time were fitted using the internal diffusion controlling reaction equation (Eq. (2)) and the chemical reaction controlling reaction equation (Eq. (3)) [27]:

$$1-2\alpha/3-(1-\alpha)^{2/3}=K_s t \quad (2)$$

$$1-(1-\alpha)^{1/3}=K_c t \quad (3)$$

where α is the leaching yield of Fe from mine waste sample; K_c and K_s are the rate constants; t is the bioleaching time.

The detailed fitting coefficients are given in Table 1. Apparently, by comparing the linear correlation coefficient (R^2), the dissolution of pyrite during bioleaching was mainly controlled by the chemical reaction process. It is worth noting that fitting result of R^2 in internal-diffusion control was very close to that of chemical reaction process, which meant that the removal of pyrite was also affected by possible secondary products formed on the surface of pyrite, such as jarosite ($(KFe_3(SO_4)_2(OH)_6)$) [28]. Jarosite was reported to be a very common secondary product during bioleaching of sulfide minerals, which was suggested to have passivation effect on the further dissolution of sulfide minerals [10].

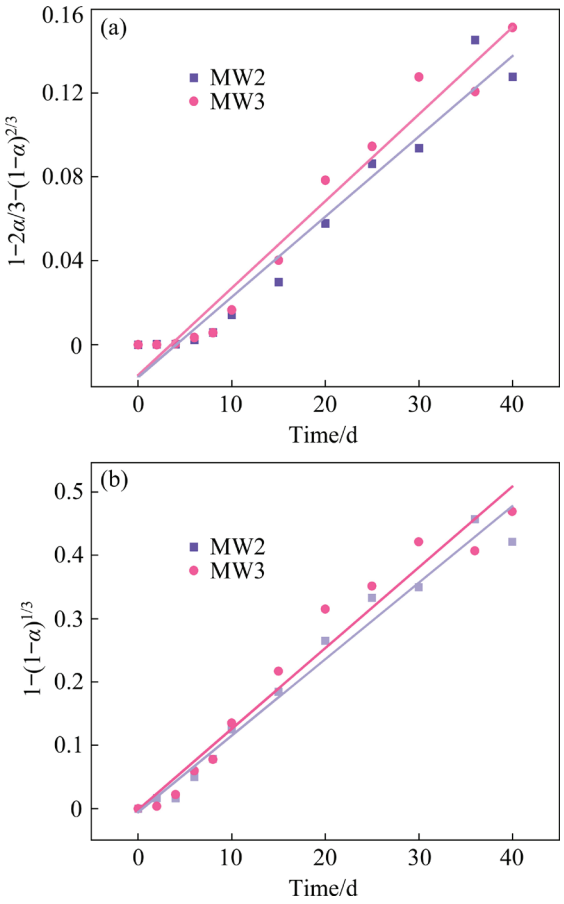

Fig. 2 Kinetics models of pyrite dissolution during bioleaching (data from Fig. 1): (a) Fitting of internal diffusion control; (b) Fitting of chemical reaction control

Table 1 Correlation coefficients of two kinetics models

Sample	$1-2\alpha/3-(1-\alpha)^{2/3}$		$1-(1-\alpha)^{1/3}$	
	R^2	K_s	R^2	K_c
MW2	0.978	3.83×10^{-3}	0.987	1.21×10^{-2}
MW3	0.980	4.15×10^{-3}	0.982	1.28×10^{-2}

3.3 Mineralogical phase analysis

XRD was conducted to investigate the mineralogical phase changes and the secondary products formation of three samples after bioleaching. The results are shown in Fig. 3. No additional phases were found in XRD pattern of residual MW1 in addition to quartz, clinochlore, dolomite, muscovite and gypsum (Fig. 3(a)). However, it was observed that the intensity of gypsum increased, which was related to the reactions between dolomite and sulfuric acid [29].

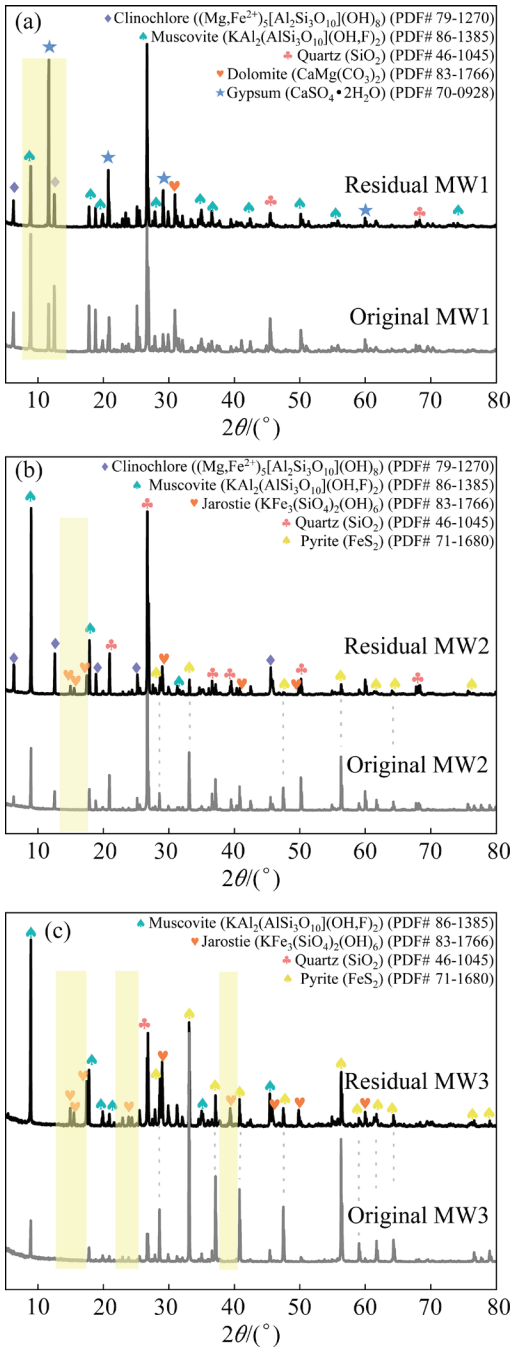

Fig. 3 XRD patterns of MW1 (a), MW2 (b) and MW3 (c) before and after bioleaching for 40 d in presence of *A. ferrooxidans*

This was also the main reason for the rapid increase in pH (Fig. 1(b)). New peaks, recognized as jarosite, were detected in the patterns of residual MW2 and MW3 (Figs. 3(b, c)), which was consistent with the deduction of the kinetics study. It has been reported that jarosite was easily formed in the presence of *A. ferrooxidans* during the bioleaching of sulfide minerals [30], which was suggested to be able to cover the surface of minerals and form a "passivation" film.

For the bioleaching of copper sulfide, the formation of jarosite is unavoidable and a nuisance, as it hinders the efficient extraction of copper [31]. However, the bio-dissolution of pyrite in nature can lead to AMD contaminating the environment, and it is more desirable to passivate pyrite [32]. Therefore, the generated jarosite may passivate the pyrite which is not totally dissolved due to the poor kinetics in the later stage of bioleaching, and thus achieve the bio-passivation of the residual pyrite. However, the morphology of jarosite is considered to be a key factor in bio-passivation, i.e., the denser the jarosite is formed, the better the bio-passivation effect is [10,33]. Thus, further characteristics are needed to determine the passivation of jarosite layer on pyrite surface.

3.4 Morphology

SEM was further carried out to verify whether the formed jarosite had a bio-passivation effect on residual pyrite. The surface morphologies of three mine waste samples (MW1, MW2 and MW3) before and after bioleaching were presented in Fig. 4. No significant change could be seen in the SEM images of original and residual MW1 (Figs. 4(a, d)), indicating that MW1 was hardly dissolved. Additionally, a large number of flaky muscovite could be observed in the original MW1 and residual MW1. Quartz and gypsum detected in XRD of MW1 could also be recognized as sharp-edged lumps and tiny sticks, respectively. However, pyrite particles were observed in the SEM image of MW2 in addition to substances detected in MW1. The surface of pyrite in original MW2 was relatively smooth with the exception of a few scrapes and defects associated with sample grinding (Fig. 4(b)). The EDS results proved that there were no other impurities on the pyrite surface (Fig. 4(g)). It was worth noting that a large number of fine and granular particles with less than 1 μm were found to be formed on the mineral surfaces in the SEM images of residual MW2 (Figs. 4(e, f)). The formation of these fine particles did not appear to be selective; it can also be found on the surfaces of other gangues, such as quartz and gypsum. The formation of jarosite layer of pyrite was mainly related to the oxidized Fe(III) on pyrite surface, while when there was an excess of Fe(III) in the

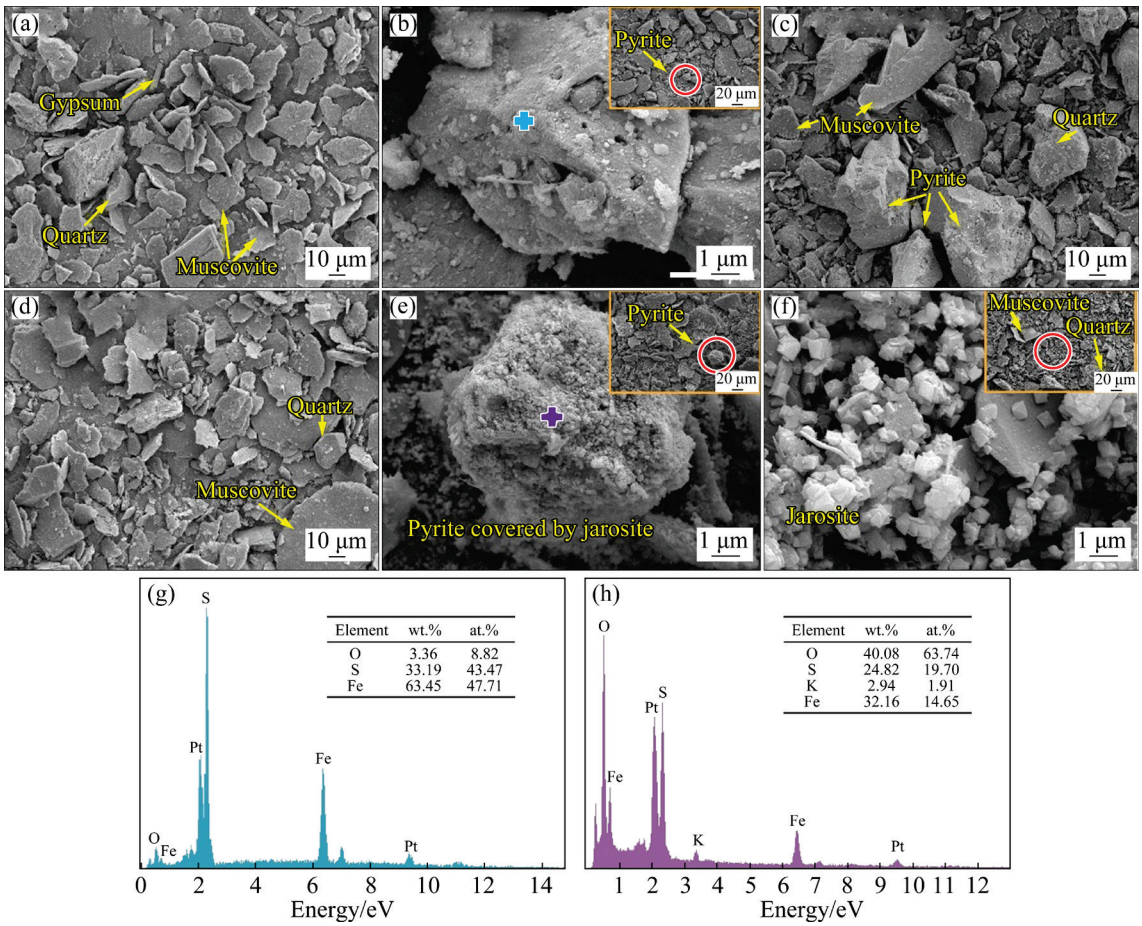

Fig. 4 SEM images of original MW1 (a), MW2 (b) and MW3 (c), residual MW1 (d), MW2 (e) and MW3 (f) after bioleaching for 40 d, and EDS results of original MW2 (g) and bioleaching residue of MW2 (h)

solution, the unsaturated O bonds on the surface of quartz and gypsum due to grinding might provide extra binding sites for the formation of jarosite.

As shown in Fig. 4(h), elements on the pyrite surface in residual MW2 at this time consisted of O, S, K and Fe with the atomic fraction of 63.74%, 19.70%, 01.91% and 14.65%, respectively, which indicated that the fine substances corresponded to the jarosite found in XRD [34], and a relatively dense layer was formed to cover the surface of pyrite. As for MW3, more pyrite particles could be found in the original SEM images (Fig. 4(c)), which was consistent with the order of pyrite content in the three samples. However, pyrite distinctly disappeared after bioleaching and was replaced by large amount of jarosite that was also observed in residual MW2, which could be proven by the results of EDS mapping in Fig. S3 in SI. The result was similar to a former study where biogenic jarosite was able to form an inhibitory layer to immobilize heavy metal from sulfide tailings [35].

3.5 Surface elemental composition

Elemental composition analysis on the surface of sample was conducted to further verify the results of XRD and SEM. Figure 5 depicts Fe 2p and S 2p spectra of the original and bioleaching residues of MW1, MW2 and MW3. Deconvolution of Fe $2p_{3/2}$ spectrum illustrated three types of Fe coordination and oxidation states present in the original and residual MW1 (Fig. 5(a)): (1) iron-oxide species (Fe(III)—O, 710−710.5 eV) [36], (2) iron−oxyhydroxide species (Fe(III) — OH, 711.4−712.5 eV) [37] and (3) iron—sulfate species (Fe(III)—S—O, 713.5−715.5 eV) [38]. Furthermore, Fe $2p_{3/2}$ peak located at 717.8−720.2 eV was attributed to the satellite peak of Fe(III) [36]. The surface iron (III) species were in relation to the clinochlore in MW1 [22]. After bioleaching for 40 d, the proportion of these iron species did not change significantly, with a slight increase in Fe(III)—O coordination and a decrease in Fe(III)—S—O and Fe(III)—OH. Four iron species, i.e., Fe(II)—S,

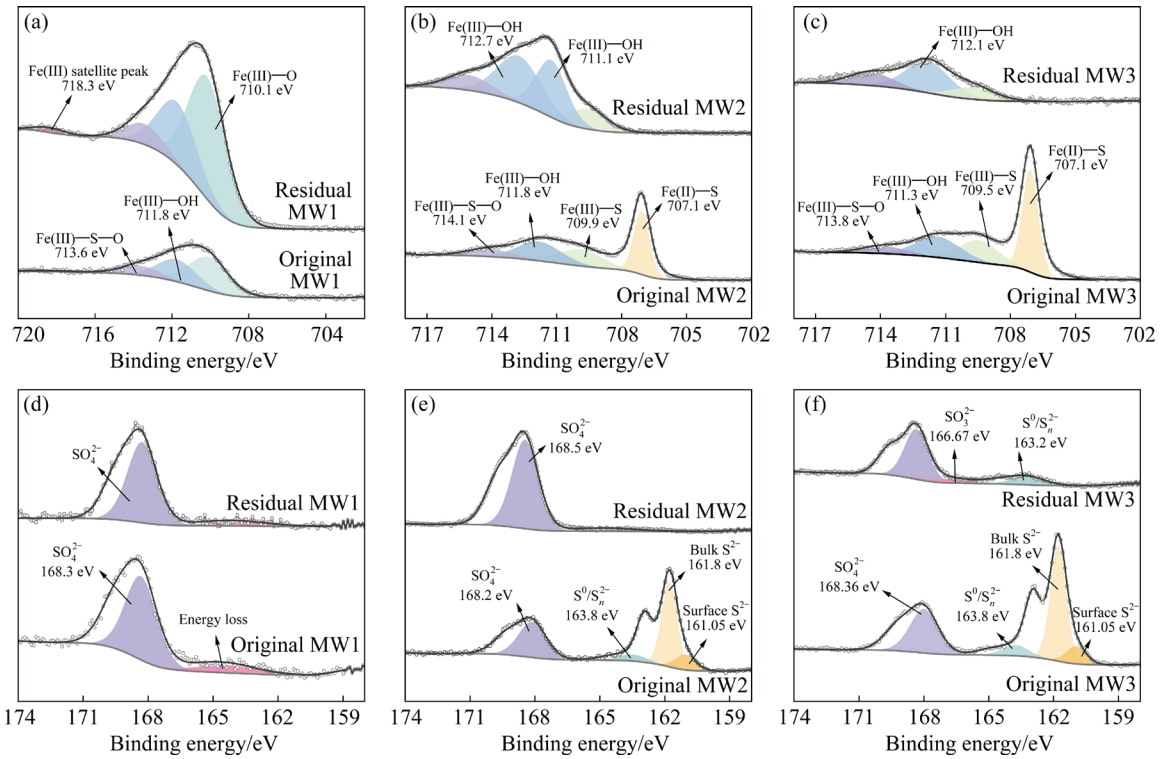

Fig. 5 XPS spectra of Fe $2p_{3/2}$ (a−c) and S $2p_{3/2}$ (d−f) of original and residual MW1 (a, d), MW2 (b, e) and MW3 (c, f) samples

Fe(III)—S, Fe(III)—OH and Fe(III)—S—O species, were fitted in the spectrum of original MW2 and MW3 (Figs. 5(b, c)). Specifically, Fe(II)—S coordination was related to the ferrous iron in bulk and on the surface of pyrite [39]. Fe(III)—S and Fe(III)—S—O structure might correspond to the oxidation of ferrous iron on the surface of pyrite. Clinochlore might be responsible for the existence of the Fe(III)—OH species [22]. On the surface of MW2 residues, the increase in Fe(III)—OH and Fe(III)—S—O proportions and decrease in Fe(III)—S proportion related to the formation of jarosite [37]. Fe(III) on pyrite surface may be bonded with jarosite, forming a passivated layer for residual pyrite. On the other hand, Fe(II)—S species could no longer be detected (Fig. S4 in SI), indicating that pyrite was largely dissolved and covered, which was consistent with the results of the bioleaching experiments and SEM observation.

As for S species on the original surface of MW1, only a sulfate peak with a binding energy of 168.5 eV was detected (Fig. 5(d)), which was attributed to the gypsum in the MW1 sample [40]. A wide peak with binding energy at 163.9−164.5 eV was reported as the energy loss feature [41]. In the bioleaching residues of MW1, S was also present in the form of SO_4^{2-} accounting for 90%, which is slightly higher than that of the original proportion (Fig. S4 in SI). This result was attributed to the formation of gypsum in MW1, which was consistent with the results of XRD. S $2p_{3/2}$ peaks with the binding energy of 161.05 and 161.8 eV were related to the surface and bulk monosulfide of pyrite, respectively (Figs. 5(e, f)) [42], which corresponded to Fe(II)—S coordination in the result of Fe $2p_{3/2}$. Elemental sulfur or polysulfide (S^0/S_n^{2-}, 163.0−164.7 eV) could be considered to be the result of slight oxidation of pyrite in original MW2 and MW3 [43,44]. Furthermore, gypsum was also responsible for SO_4^{2-} in the original MW2 and MW3. After bioleaching, S^{2-} of pyrite disappeared and SO_4^{2-} species were notably increased to account for over 93%, and 75% on the surface of residual MW2 and MW3, respectively (Fig. S4 in SI), which confirmed the dissolution of pyrite and the formation of jarosite. With the transformation of S^{2-} to the more stable SO_4^{2-}, the MW2 and MW3 would no longer produce AMD. It is worth noting that SO_3^{2-} species were detected as a new sulfur species on the residual MW, which was mainly caused by the difference in the degree of oxidation between MW2 and MW3.

3.6 AMD generation risk of leached residues

Another batch of bio-oxidation experiment was conducted on three kinds of leaching residues to examine the ability of mine waste rocks to produce AMD after bioleaching treatment. Figure 6 shows the variations in pH and total iron concentration of the three leaching residues over the period of 8 weeks biooxidation. In line with the bioleaching results of raw ore, the pH of MW1 rose to 6.0 rapidly and stabilized afterward, suggesting that the leaching residue of MW1 still had strong acid-consuming properties. The pH of the leaching residues of MW2 and MW3 was relatively stable and remained with the initial value of about 2.0 throughout the period, indicating that the acidity did not continue to be generated. According to the results in Fig. 1, about 18% of pyrite theoretically remained in the leaching residues and about 550 and 1000 mg/L total iron were not dissolved from MW2 and MW3, respectively. However, total iron concentrations in solution of MW2 and MW3 were 8 and 160 mg/L after 56 d of the experiment, indicating 98% and 84% pyrite in residual MW2 and MW3 was effectively passivated, respectively.

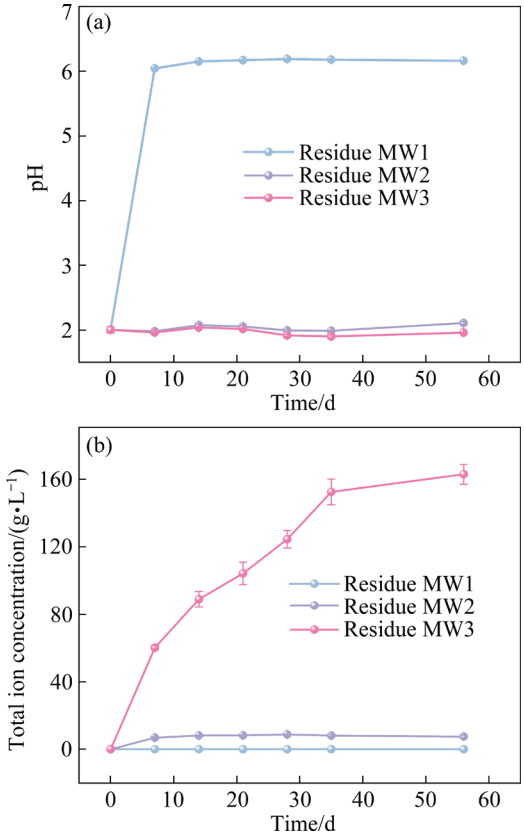

Fig. 6 Variations in pH (a) and total iron concentration (b) during bioleaching of three residue mine waste samples for another 56 d in presence of *A. ferrooxidans*

Therefore, the acid and iron release capacity of the pyrite-bearing waste rock is significantly reduced after bioleaching treatment which could reduce the risk of AMD formation for later storage.

3.7 Model and mechanism of bio-oxidation and bio-passivation for synergistic disposal of pyrite-bearing mine waste to inhibit AMD generation at source

In nature, AMD generated from pyrite-bearing waste ores is a relatively slow process, which leads to long-term persistent contamination of surrounding water bodies and soils by AMD. In contrast to previous approaches to inhibiting pyrite oxidation, a treatment was proposed in this work using bioleaching to remove pyrite from waste ores in the short term and could mitigate the risk of AMD generation, as shown in Fig. 7. During the bioleaching process, pyrite can be significantly removed in the presence of *A. ferrooxidans*. Although the pyrite is not completely removed due to the reaction kinetics, biogenic jarosite generated from ferric iron and sulfate under the mediation of *A. ferrooxidans* can passivate the surface of the residual pyrite in mine waste. Thus, bio-oxidation and bio-passivation can synergistically inhibit the subsequent AMD release from the waste rocks. With this method, the mine waste can be decontaminated without worrying about the long-term release of AMD in nature. According to the latest report, the disposal of leachate should not be a problem because it can be collected and used for bioleaching of other higher valuable minerals, such as copper sulfide [45]. Therefore, the approach can also be used to reduce the long-term operating cost of conventional AMD treatment to a certain extent.

4 Conclusions

(1) The bioleaching results showed that nearly 82% of pyrite could be removed from mine waste samples (MW2 and MW3) within 40 d. During the process, the bio-dissolution of pyrite-bearing waste ores was mainly in the control of chemical reaction as well as internal diffusion.

(2) During the bioleaching process, S^{2-} on the surface of waste ore would transform to a more stable state of SO_4^{2-}, forming biogenic jarosite on the surface of residual pyrite in mine waste.

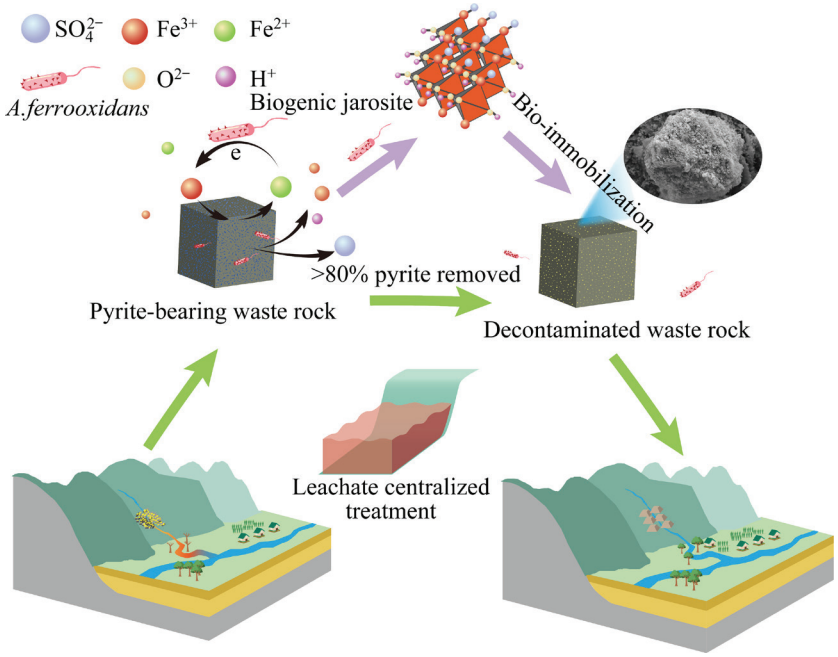

Fig. 7 Model of bio-oxidation and bio-passivation for synergistic disposal of pyrite-bearing mine waste to inhibit AMD generation at source

(3) The secondary bioleaching experiment of residue waste ore proved that the bio-passivation layer was stable and effective with only 8 and 160 mg/L Fe released from MW2 and MW3, respectively, indicating that the risk of AMD production from pyrite-bearing waste was significantly reduced.

CRediT authorship contribution statement

Mao-xin HONG: Writing − Original draft, Data curation; **Jun WANG:** Funding acquisition; **Bao-jun YANG:** Conceptualization, Investigation; **Yang LIU:** Writing − Review & editing; **Rui LIAO:** Writing − Review & editing; **Shi-chao YU:** Writing − Review & editing; **Shi-tong LIU:** Writing − Review & editing; **An-ni TANG:** Writing – Review & editing; **Wei WANG:** Writing − Review & editing; **Guan-zhou QIU:** Funding acquisition.

Declaration of competing interest

The authors declare that they have no known competing financial interests or personal relationships that could have appeared to influence the work reported in this paper.

Acknowledgments

This work was financially supported by the National Key Research and Development Program of China (Nos. 2022YFC2105300, 2022YFC2105304, 2022YFC2105305), and the Innovation-Driven Project of Central South University, China (No. 1053320220066).

Supporting Information

Supporting Information in this paper can be found at: http://tnmsc.csu.edu.cn/download/21-p2342-2023-0251-Supporting_information.pdf.

References

[1] JOHNSON D B, HALLBERG K B. Acid mine drainage remediation options: A review [J]. Science of the Total Environment, 2005, 338: 3−14.

[2] AKCIL A, KOLDAS S. Acid mine drainage (AMD): Causes, treatment and case studies [J]. Journal of Cleaner Production, 2006, 14: 1139−1145.

[3] PARK I, TABELIN C B, JEON S, LI X, SENO K, ITO M, HIROYOSHI N. A review of recent strategies for acid mine drainage prevention and mine tailings recycling [J]. Chemosphere, 2019, 219: 588−606.

[4] FAN Rong, SHORT M D, ZENG Sheng-jia, QIAN Gu-jie, LI Jun, SCHUMANN R C, KAWASHIMA N, SMART R S C, GERSON A R. The formation of silicate-stabilized passivating layers on pyrite for reduced acid rock drainage [J]. Environmental Science and Technology, 2017, 51: 11317−11325.

[5] LIAO Rui, YANG Bao-jun, HUANG Xiao-tao, HONG Mao-xin, YU Shi-chao, LIU Shi-tong, WANG Jun, QIU Guan-zhou. Combined effect of silver ion and pyrite on AMD formation generated by chalcopyrite bio-dissolution [J]. Chemosphere, 2021, 279: 130516.

[6] GUPTA V, COURTEMANCHE J, GUNN J, MYKYTCZUK N. Shallow floating treatment wetland capable of sulfate reduction in acid mine drainage impacted waters in a northern climate [J]. Journal of Environmental Management, 2020, 263: 110351.

[7] CHEN Guan, YE Yi-cheng, YAO Nan, HU Nan-yan, ZHANG Jie, HUANG Yang. A critical review of prevention, treatment, reuse, and resource recovery from acid mine drainage [J]. Journal of Cleaner Production, 2021, 329: 129666.

[8] QIAN Gu-jie, FAN Rong, SHORT M D, SCHUMANN R C, PRING A, GERSON A R. The combined effects of galvanic interaction and silicate addition on the oxidative dissolution of pyrite: Implications for acid and metalliferous drainage control [J]. Environmental Science and Technology, 2019, 53: 11922−11931.

[9] SANCHEZ-ANDREA I, SANZ J L, BIJMANS M F, STAMS A J. Sulfate reduction at low pH to remediate acid mine drainage [J]. Journal of Hazardous Materials, 2014, 269: 98−109.

[10] YANG Bao-jun, LIN Mo, FANG Jing-hua, ZHANG Rui-yong, LUO Wen, WANG Xing-xing, LIAO Rui, WU Bai-qiang, WANG Jun, GAN Min, LIU Bin, ZHANG Yi, LIU Xue-duan, QIN Wen-qing, QIU Guan-zhou. Combined effects of jarosite and visible light on chalcopyrite dissolution mediated by *Acidithiobacillus ferrooxidans* [J]. Science of the Total Environment, 2020, 698: 134175.

[11] COZZOLINO D, CHANDRA S, ROBERTS J, POWER A, RAJAPAKSHA P, BALL N, GORDON R, CHAPMAN J. There is gold in them hills: Predicting potential acid mine drainage events through the use of chemometrics [J]. Science of the Total Environment, 2018, 619/620: 1464−1472.

[12] ZHAO Chun-xiao, YANG Bao-jun, WANG Xing-xing, ZHAO Hong-bo, GAN Min, QIU Guan-zhou, WANG Jun. Catalytic effect of visible light and Cd^{2+} on chalcopyrite bioleaching [J]. Transactions of Nonferrous Metals Society of China, 2020, 30: 1078−1090.

[13] YANG Bao-jun, LUO Wen, LIAO Qi, ZHU Jian-yu, GAN Min, LIU Xue-duan, QIU Guan-zhou. Photogenerated-hole scavenger for enhancing photocatalytic chalcopyrite bioleaching [J]. Transactions of Nonferrous Metals Society of China, 2020, 30: 200−211.

[14] ZHAO Hong-bo, WANG Jun, QIN Wen-qing, ZHENG Xi-hua, TAO Lang, GAN Xiao-wen, QIU Guan-zhou. Surface species of chalcopyrite during bioleaching by moderately thermophilic bacteria [J]. Transactions of Nonferrous Metals Society of China, 2015, 25: 2725−2733.

[15] WANG Jun, ZHAO Hong-bo, ZHUANG Tian, QIN Wen-qing, ZHU Shan, QIU Guan-zhou. Bioleaching of Pb−Zn−Sn chalcopyrite concentrate in tank bioreactor and microbial community succession analysis [J]. Transactions of Nonferrous Metals Society of China, 2013, 23: 3758−3762.

[16] HONG Mao-xin, LIN Hao, YANG Bao-jun, XIAO Jing, LIAO Rui, YU Shi-cchao, ZHAO Chun-xiao, LIU Shi-tong, SUN Xin, WANG Jun, QIU Guan-zhou. Evolution of passivating species on bornite surface during electrochemical dissolution [J]. Transactions of Nonferrous Metals Society of China, 2023, 33: 1906−1918.

[17] NGUYEN T H, WON S, HA M G, NGUYEN D D, KANG H Y. Bioleaching for environmental remediation of toxic metals and metalloids: A review on soils, sediments, and mine tailings [J]. Chemosphere, 2021, 282: 131108.

[18] MÄKINEN J, SALO M, KHOSHKHOO M, SUNDKVIST J E, KINNUNEN P. Bioleaching of cobalt from sulfide mining tailings: A mini-pilot study [J]. Hydrometallurgy, 2020, 196: 105418.

[19] YE Mao-you, LIANG Jia-lin, LIAO Xiao-jian, LI Li-li, FENG Xi-dan, QIAN Wei, ZHOU Si-yu, SUN Shui-yu. Bioleaching for detoxification of waste flotation tailings: Relationship between EPS substances and bioleaching behavior [J]. Journal of Environmental Management, 2021, 279: 111795.

[20] RODRÍGUEZ Y, BALLESTER A, BLÁZQUEZ M L, GONZÁLEZ F, MUÑOZ J A. New information on the pyrite bioleaching mechanism at low and high temperature [J]. Hydrometallurgy, 2003, 71: 37−46.

[21] YANG Bao-jun, ZHAO Chun-xiao, LOU Wen, LIAO Rui, GAN Min, WANG Jun, LIU Xue-duan, QIU Guan-zhou. Catalytic effect of silver on copper release from chalcopyrite mediated by *Acidithiobacillus ferrooxidans* [J]. Journal of Hazardous Materials, 2020, 392: 122290.

[22] LU Zhi-yun, HE Xue-mei, LIN Chen-lu, LIANG Lin, JIN Xin-yu, GUO Qing-feng. Color and genesis of californite from Pakistan: Insights from μ-XRF mapping, optical spectra and X-ray photoelectron spectroscopy [J]. Scientific Reports, 2020, 10: 285.

[23] DESCOSTES M, VITORGE P, BEAUCAIRE C. Pyrite dissolution in acidic media [J]. Geochimica et Cosmochimica Acta, 2004, 68: 4559−4569.

[24] ZHAO Hong-bo, WANG Jun, QIN Wen-qing, HU Ming-hao, ZHU Shan, QIU Guan-zhou. Electrochemical dissolution process of chalcopyrite in the presence of mesophilic microorganisms [J]. Minerals Engineering, 2015, 71: 159−169.

[25] QUATRINI R, JOHNSON D B. *Acidithiobacillus ferrooxidans* [J]. Trends in Microbiology, 2019, 27: 282−283.

[26] LIAO Rui, WANG Xing-xing, YANG Bao-jun, HONG Mao-xin, ZHAO Hong-bo, WANG Jun, QIU Guan-zhou. Catalytic effect of silver-bearing solid waste on chalcopyrite bioleaching: A kinetic study [J]. Journal of Central South University, 2020, 27: 1395−1403.

[27] ZHANG Li-juan, ZHOU Wen-bo, LIU Yong-di, JIA Hong-hua, ZHOU Jun, WEI Ping, ZHOU Hong-bo. Bioleaching of dewatered electroplating sludge for the extraction of base metals using an adapted microbial consortium: Process optimization and kinetics [J]. Hydrometallurgy, 2020, 191: 105227.

[28] ZHAO Hong-bo, ZHANG Yi-sheng, ZHANG Xian, QIAN Lu, SUN Meng-lin, YANG Yu, ZHANG Yan-sheng, WANG Jun, KIM H, QIU Guan-zhou. The dissolution and passivation mechanism of chalcopyrite in bioleaching: An overview [J]. Minerals Engineering, 2019, 136: 140−154.

[29] EL-MIDANY A A, EL-SHALL H, SVORONOS S. Modeling the PVA-coated dolomite floatability in acidic media [J]. Powder Technology, 2011, 209: 25−28.

[30] HONG Mao-xin, LIU Shi-tong, HUANG Xiao-tao, YANG Bao-jun, ZHAO Chun-xiao, YU Shi-chao, LIU Yu-ling, QIU Guan-zhou, WANG Jun. A review on bornite (bio)leaching [J]. Minerals Engineering, 2021, 174: 107245.

[31] WANG Jun, GAN Xiao-wen, ZHAO Hong-bo, HU Ming-hao, LI Kai-yun, QIN Wen-qing, QIU Guan-zhou. Dissolution and passivation mechanisms of chalcopyrite during bioleaching: DFT calculation, XPS and electro-

chemistry analysis [J]. Minerals Engineering, 2016, 98: 264−278.
[32] TU Zhi-hong, WU Qi, HE Hong-ping, ZHOU Shu, LIU Jie, HE Hui-jun, LIU Chong-min, DANG Zhi, REINFELDER J R. Reduction of acid mine drainage by passivation of pyrite surfaces: A review [J]. Science of the Total Environment, 2022, 832: 155116.
[33] ZHANG Lin, QIU Guan-zhou, HU Yue-hua, SUN Xiao- jun, LI Jian-hua, GU Guo-hua. Bioleaching of pyrite by *A. ferrooxidans* and *L. ferriphilum* [J]. Transactions of Nonferrous Metals Society of China, 2008, 18: 1415−1420.
[34] ZHU Jian-yu, GAN Min, ZHANG Dan, HU Yue-hua, CHAI Li-yuan. The nature of schwertmannite and jarosite mediated by two strains of *Acidithiobacillus ferrooxidans* with different ferrous oxidation ability [J]. Material Science Engineering C, 2013, 33: 2679−2685.
[35] PIERVANDI Z, KHODADADI DARBAN A, MOUSAVI S M, ABDOLLAHY M, ASADOLLAHFARDI G, FUNARI V, DINELLI E, WEBSTER R D, SILLANPAA M. Effect of biogenic jarosite on the bio-immobilization of toxic elements from sulfide tailings [J]. Chemosphere, 2020, 258: 127288.
[36] GAN Min, SUN Sheng-jie, ZHENG Zhi-he, TANG Hao-jia, SHENG Jing-rui, ZHU Jian-yu, LIU Xing-xing. Adsorption of Cr(VI) and Cu(II) by $AlPO_4$ modified biosynthetic Schwertmannite [J]. Applied Surface Science, 2015, 356: 986−997.
[37] ZHAO Chun-xiao, YANG Bao-jun, LIAO Rui, HONG Mao-xin, YU Shi-chao, LIU Shi-tong, WANG Jun, QIU Guan-zhou. Combined effect and mechanism of visible light and Ag^+ on chalcopyrite bioleaching [J]. Minerals Engineering, 2022, 175: 107283.
[38] OUYANG Bing-jie, LU Xian-cai, LIU Huan, LI Juan, ZHU Ting-ting, ZHU Xiang-yu, LU Jian-jun, WANG Ru-cheng. Reduction of jarosite by *Shewanella oneidensis* MR-1 and secondary mineralization [J]. Geochimica et Cosmochimica Acta, 2014, 124: 54−71.
[39] KIM E J, BATCHELOR B. Macroscopic and X-ray photoelectron spectroscopic investigation of interactions of arsenic with synthesized pyrite [J]. Environmental Science & Technology, 2009, 43: 2899−2904.
[40] ZHANG Zhi-guo, CAO Yi-jun, LIAO Yin-fei, MA Zi-long. Study on comparison adsorption of calcium and sulfate on scheelite and fluorite surfaces [J]. Separation Science and Technology, 2018, 54: 1247−1256.
[41] LI Yu-biao, KAWASHIMA N, LI J, CHANDRA A P, GERSON A R. A review of the structure, and fundamental mechanisms and kinetics of the leaching of chalcopyrite [J]. Advances in Colloid & Interface Science, 2013, 197/198: 1−32.
[42] ZHAO Chun-xiao, YANG Bao-jun, LIAO Rui, HONG Mao-xin, YU Shi-chao, WANG Jun, QIU Guan-zhou. Catalytic mechanism of manganese ions and visible light on chalcopyrite bioleaching in the presence of *Acidithiobacillus ferrooxidans* [J]. Chinese Journal of Chemical Engineering, 2021, 41: 457−465.
[43] HONG Mao-xin, WANG Xing-xing, YANG Bao-jun, LIU Shi-tong, LIN Hao, QIU Guan-zhou, QIN Wen-qing, WANG Jun. Effect of pyrite with different semiconducting properties on bornite bioleaching in the presence of *Leptospirillum ferriphilum* [J]. Hydrometallurgy, 2020, 196: 105414.
[44] LIU Shi-tong, HONG Mao-xin, WANG Xing-xing, YANG Bao-jun, LIN Hao, LIN Mo, WANG Jun, QIU Guan-zhou. Pretreatment with acidic ferric sulfate leaching promotes the bioleaching of bornite [J]. Hydrometallurgy, 2020, 196: 105349.
[45] HONG Mao-xin, WANG Wei, LI Lai-shun, LIU Yang TONG Li-zhi, QIU Guan-zhou, YANG Bao-jun, WANG Jun. The use of biogenic Fe^{3+} and H_2SO_4 generated from pyrite waste to enhance bornite bioleaching: A potential utilization of acid mine drainage [J]. Minerals Engineering, 2022, 190: 107927.

嗜酸氧化亚铁硫杆菌作用下含黄铁矿废石的生物溶解和动力学

洪茂鑫[1,2]，王 军[1,2]，杨宝军[1,2]，刘 洋[1,2]，廖 彗[1,2]，
于世超[1,2]，刘仕统[1,2]，汤安妮[1,2]，王 炜[1,3]，邱冠周[1,2]

1. 中南大学 资源加工与生物工程学院，长沙 410083；
2. 中南大学 生物冶金教育部重点实验室，长沙 410083；
3. 生态环境部华南环境科学研究所，广州 510655

摘 要：使用生物淋洗处理黄铁矿废石，从源头上缓解其产生酸性矿山废水(AMD)的风险。生物淋洗结果显示，在嗜酸氧化亚铁硫杆菌(*A. ferrooxidans*)的作用下，40 天内可以从黄铁矿废石中去除近 82%的铁和硫。动力学研究结果表明，废石中黄铁矿的去除主要受化学反应和内扩散控制。X 射线衍射(XRD)和 X 射线光电子能谱(XPS)的结果表明，在 *A. ferrooxidans* 细菌介导下，生物源黄钾铁矾能够钝化废石中残余的黄铁矿。对渣样进行二次生物浸出，试验发现溶液 pH 没有明显下降，且仅有 8 mg/L 和 160 mg/L 的铁从两个黄铁矿废石渣样中溶出，表明渣样的酸和铁释放能力得到削弱。

关键词：酸性矿山废水；黄铁矿；生物浸出；矿山废弃物；黄钾铁矾；生物钝化

(Edited by Bing YANG)